Single-detector polarization-sensitive optical frequency domain imaging using high-speed intra A-line polarization modulation

W. Y. Oh, B. J. Vakoc, S. H. Yun, G. J. Tearney, and B. E. Bouma

Harvard Medical School and Wellman Center for Photomedicine, Massachusetts General Hospital, 50 Blossom Street, BAR 704, Boston, Massachusetts 02114, USA
**Corresponding author: woh1@partners.org*

Received February 5, 2008; revised April 9, 2008; accepted April 22, 2008; posted May 7, 2008 (Doc. ID 92481); published June 12, 2008

We demonstrate a novel high-speed polarization-sensitive optical frequency domain imaging system employing high-speed polarization modulation. Rapid and continuous polarization modulation of light prior to illumination of the sample is accomplished by shifting the frequency of one polarization eigenstate by an amount equal to one quarter of the digitization sampling frequency. This approach enables polarization-sensitive imaging with a single detection channel and overcomes artifacts that may arise from temporal variations of the birefringence in fiber-optic imaging probes and spatial variation of birefringence in the sample. © 2008 Optical Society of America

OCIS codes: 170.4500, 170.3880, 170.3890.

Polarization-sensitive optical coherence tomography (PS-OCT) [1,2] is a technique for quantifying and visualizing the distribution of birefringence in samples. This capability is relevant to a wide spectrum of biomedical applications and is particularly useful for diagnosing pathology and characterizing injury in clinical medicine [3,4]. Although ophthalmic [3] and dermatologic [4] applications of PS-OCT are perhaps the most mature, recent preclinical work has demonstrated that PS-OCT can quantify collagen content and smooth muscle cell density in atherosclerotic plaques *ex vivo* [5]. Performing these measurements *in vivo* simultaneously with catheter-based [6] high-speed optical frequency domain imaging (OFDI) [7,8] could greatly advance the understanding of coronary atherosclerosis and acute myocardial infarction in humans.

In conventional fiber-optic PS-OCT, polarization-diverse detection and polarization modulation are implemented to measure birefringence properties of the tissue sample. Polarization-diverse detection determines Stokes vector components of the light reflected from each depth of the tissue by measuring projections onto a pair of orthogonal polarization states through a polarization beam splitter (PBS) and two detection channels. Since two input polarization states perpendicular to each other on the Poincaré sphere are required for the determination of the optic axis and phase retardation in the tissue with any arbitrary static birefringence of the sample arm optical fiber, the polarization state of the light incident on the sample is modulated between two perpendicular states on the Poincaré sphere on successive axial scans (A-lines) [2]. A single axial birefringence profile of the sample is then provided from the Stokes vectors obtained with two perpendicular polarization input states via either Stokes vector analysis [9] or Jones matrix analysis [10].

However, in high-speed intracoronary imaging through a rapidly spinning catheter, birefringence images are prone to artifacts that can arise from rapid stress-induced birefringence changes in the fiber-optic catheter that occur during the time interval between successive A-lines [11]. Much faster polarization modulation or simultaneous detection of these two perpendicular polarization states can overcome such artifacts. Polarization-sensitive optical frequency domain imaging (PS-OFDI) with a frequency-multiplexing scheme that enables simultaneous illumination and detection of a pair of perpendicular polarization states on the Poincaré sphere was recently proposed, and high-speed polarization-sensitive imaging of human coronary arteries *ex vivo* using a rotational fiber-optic catheter was demonstrated [12]. As in the conventional PS-OCT and PS-OFDI approaches, however, the frequency-multiplexed configuration requires careful orientation of the polarization eigenstates and two separate detectors for polarization-diverse and polarization-sensitive imaging. In this Letter, we demonstrate a new PS-OFDI scheme that modulates the sample arm polarization at a rate comparable to the digitizer sampling frequency, more than 2 orders of magnitude faster than in conventional PS-OCT, and provides artifact-free polarization-sensitive imaging. The novel modulation scheme also allows detection of all Stokes components of the light reflected from the sample using only a single detection channel without polarization diversity, thereby significantly reducing the complexity of the optical receiver.

In the OFDI with high-speed polarization modulation scheme, Fig. 1, the sample arm polarization state is continuously rotated on the Poincaré sphere. This is accomplished conveniently by frequency shifting one polarization eigenstate; the input PBS of the sample arm Mach–Zehnder interferometer (MZI) divides the input beam into two orthogonal polarization states, and an acousto-optic frequency shifter modulates one state prior to recombination. This results in a continuous rotation of the sample arm po-

0146-9592/08/121330-3/$15.00

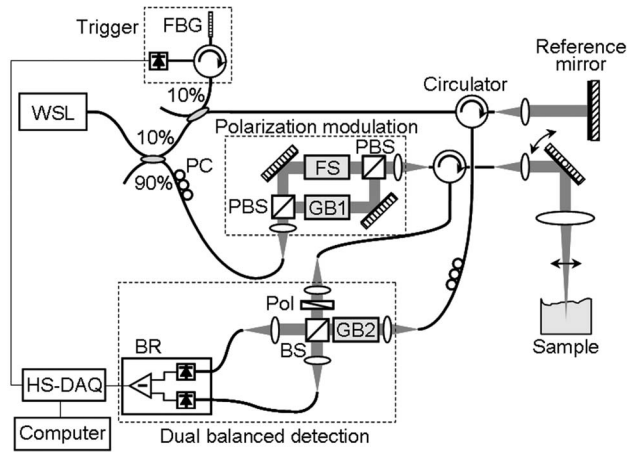

Fig. 1. Schematic of the PS-OFDI system. FBG, fiber Bragg grating; PC, polarization controller; PBS, polarization beam splitter; FS, frequency shifter; GB, AMTIR glass block; Pol, polarizer; BS, beam splitter; BR, balanced receiver, HS-DAQ, high-speed digitizer.

larization at a rate equal to the magnitude of the frequency shift. When the modulation frequency is set to a quarter of the sampling rate of the data acquisition, the output polarization of the MZI circumnavigates the Poincaré sphere once in every four sampling periods as described in Fig. 2. A single digitized A-line is then time demultiplexed into four sets of A-lines: x_i, $\tilde{x}_i$, y_i, and $\tilde{y}_i$. Each of these demodulated A-lines is associated with states of polarization equally spanning a great circle on the Poincaré sphere and is separately processed according to conventional OFDI methods [7]. The odd data sets, x_i and y_i in Fig. 2, correspond to measurements with two orthogonal polarization inputs and are used to determine a set of Stokes vectors. Another set of Stokes vectors was obtained in the same way with the even data set, $\tilde{x}_i$ and $\tilde{y}_i$. A single axial profile of birefringence was then obtained from these two sets of Stokes vector components, which are perpendicular to each other on the Poincaré sphere. Since the polarization modulation speed of this scheme is hundreds of times faster than that of conventional PS-OCT or PS-OFDI, artifacts due to time-dependent birefringence changes of the fiber-optic components, such as the catheter, can be significantly reduced.

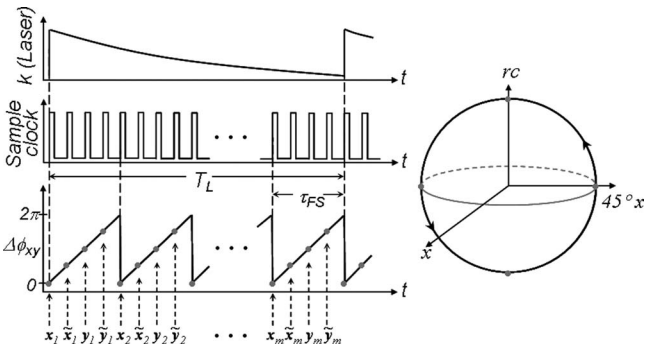

Fig. 2. Phase plot and the Poincaré sphere representation. The parameter $\Delta\phi_{xy}$ represents the phase difference between orthogonal components of the light polarization incident on the sample. Gray dots in the phase plot and the Poincaré sphere representation show the polarization states on the sample when the digitizer acquires data; $\Delta\phi_{xy} = \mathrm{mod}[|\phi_x - \phi_y|]$.

As shown in Fig. 1, a wavelength-swept laser employing a polygon scanning filter was used as a light source for the system, providing a wavelength sweep range of 1245–1355 nm with a continuously variable repetition rate of up to 100 kHz and an instantaneous linewidth of 0.11 nm. The average output power of the polarized light source was 51 mW. Ninety percent of the laser output was coupled to the sample arm of the system interferometer, where it was further divided into two orthogonal polarization states with a PBS. One of the polarization states experienced a frequency shift of 50 MHz (Brimrose, Inc., AMF-50-1300, 50 MHz), and the other polarization state passed through an AMTIR glass block that provides the same amount of chromatic dispersion as the frequency shifter. The two polarization states were then recombined with a second PBS, resulting in a polarization state that circumnavigates the Poincaré sphere at a constant rate of 50 MHz. Light reflected from the sample was polarized using a linear polarization and then combined with the reference arm light using a 50/50 beam splitter. Source relative intensity noise and autocorrelation noise were suppressed with a balanced receiver (Thorlabs PDB110C, 100 MHz), and the receiver output was digitized with a high-speed and high-resolution data acquisition board (National Instruments PCI-5124, 200 MS/s, 12 bits).

Each of the four demodulated A-lines occupied a signal band from 0 to 25 MHz with the zero frequency corresponding to the zero delay depth, and the sampling rate for each demodulated A-line was 50 MHz (one quarter of the native acquisition sampling of 200 MS/s), ensuring Nyquist sampling as described. Considering these parameters, operation of the laser at its maximum repetition rate of 100 kHz would provide a ranging depth of 1.9 mm. For the purpose of demonstration, the laser was operated at a repetition rate of 50 kHz, corresponding to a ranging depth of 3.8 mm, which is comparable to the single-sided coherence length of the laser of 3.6 mm (0.10 nm instantaneous linewidth at 50 kHz). The sensitivity of the system was measured to be 108 dB near zero delay.

Intensity and phase retardation images of a chicken leg muscle tissue *ex vivo* are shown in Figs. 3(a) and 3(b), respectively. The images comprise 504 A-lines and span 10 mm in transverse extent and 3.6 mm in depth. While the intensity image shows relatively homogeneous structures in the sample, the periodic axial banding structure was observed in the phase retardation image, showing the existence of strong birefringence in the tissue. By taking into account the rotational direction of the Stokes vectors on the Poincaré sphere in the Stokes vector analysis [9], phase unwrapping was performed as depicted in Fig. 3(c) [10]. A swine coronary artery was also imaged through the rapidly spinning fiber-optic catheter at a rate of 100 rps *ex vivo* as shown in Fig. 4. As expected, periodic circumferential artifacts that could

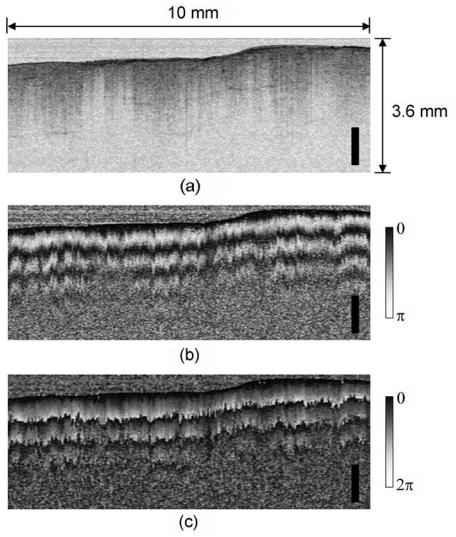

Fig. 3. (a) Intensity, (b) phase retardation, and (c) unwrapped phase retardation images of chicken muscle *ex vivo*. Scale bar, 1 mm.

result from stress-induced birefringence variations in the fiber-optic probe are not observed in the phase retardation image.

Although not demonstrated here, we note that the high-speed modulation approach to PS-OFDI is compatible with previously demonstrated methods to remove frequency degeneracy between positive and negative delays [13]. For example, a 25 MHz frequency shifter could be used in the reference arm to offset the zero delay depth point to 25 MHz. In this case, the signal bandwidth would become 50 MHz, and the sampling rate for each demodulated A-line, which is equivalent to the sample arm frequency shift, should be increased to 100 MHz for Nyquist sampling, resulting in a native digitization rate of 400 MS/s on a single channel.

In conclusion, we have demonstrated a novel high-speed PS-OFDI scheme based on rapid polarization modulation. This approach is unique in that it allows a full determination of the Stokes components with a single-detector and a single data acquisition channel, thus significantly reducing the complexity of the optical receiver. Spectral-domain PS-OCT could also potentially benefit from this scheme by implementing the four-step polarization modulation and using a single spectrometer camera for simplification of the system design and cost reduction, although lateral oversampling would be required to maintain the phase sensitivity for an accurate Stokes vector determination [14]. OFDI systems that utilize one data acquisition channel for recalibration of nonlinear wavelength tuning can also utilize the proposed scheme, since polarization-sensitive imaging can be achieved with a single detection channel [15].

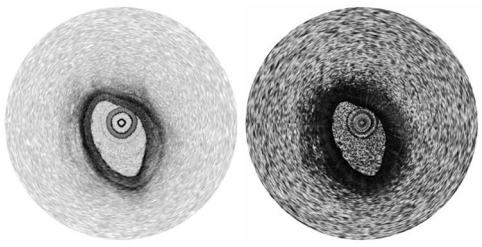

Fig. 4. Intensity and phase retardation images of a swine coronary artery *ex vivo* acquired through the rapidly spinning fiber-optic catheter.

This research was supported in part by the U.S. National Institutes of Health (contract RO1 HL076398) and by the Terumo Corporation.

References

1. M. R. Hee, D. Huang, E. A. Swanson, and J. G. Fujimoto, J. Opt. Soc. Am. B **9**, 903 (1992).
2. C. E. Saxer, J. F. de Boer, B. H. Park, Y. H. Zhao, Z. P. Chen, and J. S. Nelson, Opt. Lett. **25**, 1355 (2000).
3. B. Cense, T. C. Chen, B. H. Park, M. C. Pierce, and J. F. de Boer, Opt. Lett. **27**, 1610 (2002).
4. J. Strasswimmer, M. C. Pierce, B. H. Park, V. Neel, and J. F. de Boer, J. Biomed. Opt. **9**, 292 (2004).
5. S. Nadkarni, M. C. Pierce, B. H. Park, J. F. de Boer, E. F. Halpern, S. L. Houser, B. E. Bouma, and G. J. Tearney, J. Am. Coll. Cardiol. **49**, 1474 (2007).
6. S. H. Yun, G. J. Tearney, B. J. Vakoc, M. Shishkov, W. Y. Oh, A. E. Desjardins, M. J. Suter, R. C. Chan, J. A. Evans, I. K. Jang, N. S. Nishioka, J. F. de Boer, and B. E. Bouma, Nat. Med. **12**, 1429 (2006)
7. S. H. Yun, G. J. Tearney, J. F. de Boer, N. Iftimia, and B. E. Bouma, Opt. Express **11**, 2953 (2003).
8. W. Y. Oh, S. H. Yun, B. J. Vakoc, G. J. Tearney, and B. E. Bouma, Appl. Phys. Lett. **88**, 103902 (2006).
9. B. H. Park, M. C. Pierce, B. Cense, and J. F. de Boer, Opt. Express **11**, 782 (2003).
10. B. H. Park, M. C. Pierce, B. Cense, and J. F. de Boer, Opt. Lett. **29**, 2512 (2004).
11. M. C. Pierce, M. Shishkov, B. H. Park, N. A. Nassif, B. E. Bouma, G. J. Tearney, and J. F. de Boer, Opt. Express **13**, 5739 (2005).
12. W. Y. Oh, S. H. Yun, B. J. Vakoc, M. Shishkov, A. E. Desjardins, B. H. Park, J. F. de Boer, G. J. Tearney, and B. E. Bouma, Opt. Express **16**, 1096 (2008).
13. S. H. Yun, G. J. Tearney, J. F. de Boer, and B. E. Bouma, Opt. Express **12**, 4822 (2004).
14. B. H. Park, M. C. Pierce, B. Cense, S. H. Yun, M. Mujat, G. J. Tearney, B. E. Bouma, and J. F. de Boer, Opt. Express **13**, 3931 (2005).
15. R. Huber, M. Wojtkowski, and J. G. Fujimoto, Opt. Express **17**, 3225 (2006).